

Revealing Excitonic and Electron-Hole Plasma States in Stimulated Emission of Single CsPbBr₃ Nanowires at Room Temperature

Mai He¹, Ying Jiang,¹ Qingbo Liu,¹ Ziyu Luo,² Chenxing Ouyang,¹ Xiaoxia Wang,¹ Weihao Zheng,¹ Kai Braun,³ Alfred J. Meixner,³ Tingge Gao,^{4,5} Xiao Wang^{1,*} and Anlian Pan^{1,2,†}

¹Key Laboratory for Micro-Nano Physics and Technology of Hunan Province, School of Physics and Electronics, Hunan University, Changsha 410012, China

²Key Laboratory for Micro-Nano Physics and Technology of Hunan Province, College of Materials Science and Engineering, Hunan University, Changsha 410012, China

³Institute of Physical and Theoretical Chemistry and LISA+, University of Tübingen, Auf der Morgenstelle 18, 72076 Tübingen, Germany

⁴Tianjin Key Laboratory of Molecular Optoelectronic Science, Institute of Molecular Plus, Tianjin University, Tianjin 300072, China

⁵Department of Physics, School of Science, Tianjin University, Tianjin 300072, China



(Received 19 October 2019; revised manuscript received 24 March 2020; accepted 8 April 2020; published 28 April 2020)

Nanostructured lead halide perovskites have received extensive attention due to their potential applications in integrated photonics. Despite many successful realizations of nanoscale coherent-light sources from lead halide perovskites, the role and interplay between excitonic and electron-hole plasma (EHP) states in the stimulated-emission process are not demonstrated yet. In this work, the carrier behavior and dynamics of the stimulated emission in CsPbBr₃ single nanowires are studied with a streak camera under power-dependent one-photon and two-photon excitation at room temperature. A redshift of the lasing gain profile with increasing excitation fluence is observed, suggesting the transition from the excitonic state to EHP state that is responsible for the lasing. Whereas, a blueshift of the gain profile with time decay represents the opposite direction of the former process. Moreover, the individual lasing modes show a blueshift as excitation fluence increases and a redshift as time elapses, due to the carrier-density dependence of the refractive index. This study could provide a comprehensive and deeper understanding of the carrier-density-driven stimulated-emission dynamics in lead halide nanowires and extend their applications in integrated photonics.

DOI: 10.1103/PhysRevApplied.13.044072

I. INTRODUCTION

In recent years, lead halide perovskites have been among the most promising materials in optoelectronics and photonics with fascinating applications ranging from photovoltaic systems [1,2] to light-emitting diodes [3,4]. Nanostructured lead halide perovskites, such as nanowires [5,6], nanorods [7], and nanoplates [8], have been reported as nanoscale efficient and even coherent-light sources based on the cavity formed by themselves, which have great potential in integrated photonics due to the intrinsic high quantum efficiency and low threshold [9–13]. Furthermore, the optical properties of nanostructured lead halide perovskites can be largely tuned by varying the halide compositions, making the photonic applications covering the whole visible and also near infrared ranges

[7,14,15]. On the other hand, the lead halide perovskites with unique dielectric function, crystal-liquid duality, and defect tolerance [16,17], provide a perfect platform for fundamental studies of carrier properties and the related photophysics [18]. A full understanding of carrier behaviors in lead halide perovskites, especially, highly dense optical generated carriers and their dynamics in a self-formed cavity, could help to extend the photonics and optoelectronics applications.

In semiconductor nanostructures, excitons exist with binding energies larger than the thermal energy and are in general strongly emissive. Stimulated emission can originate from the excitonic state in semiconductor nanowires, e.g., CdS nanowires [19]. However, in the high exciton density regime (above the critical Mott density), when the average exciton distance r is comparable to its Bohr radius a_{Bohr} , excitons become unstable due to the screening of Coulomb attraction and cannot be considered as individual quasiparticles such that a new

*xiao_wang@hnu.edu.cn

†anlian.pan@hnu.edu.cn

collective phase electron-hole plasma (EHP) is formed [20,21]. This normally occurs in semiconductors under strong pulsed lasing excitation. The EHP formation and stimulated emission from EHP state in ZnO nanostructures have been reported [22–27]. EHP can also be formed in lead halide perovskites [28], and lasing from EHP state under strong pulsed excitation at liquid nitrogen temperature was demonstrated with Kerr gating technique very recently [29]. Despite many successful realizations of nanoscale lasing and underlying lasing-mechanism studies in lead halide perovskites, the interplay between excitonic and EHP states and a possible transition from these two states during the stimulated-emission process is not demonstrated yet.

In this work, we report a systematical investigation of carrier-density-dependent one- and two-photon pumped-lasing dynamics in CsPbBr₃ single nanowires by time-resolved emission spectroscopy with a streak camera at room temperature. Lasing can be achieved in a single CsPbBr₃ nanowire that serves as both the gain material and the cavity. For different excitation conditions, we record the time evolution of the stimulated-emission spectra, revealing the peak shift of individual lasing modes and the whole lasing gain profile as a function of the excitation fluence and the time decay. The role and interplay between excitonic and EHP states in the lasing process are studied. This work provides a comprehensive and deeper understanding of the lasing mechanism and dynamics in lead halide nanostructures.

II. EXPERIMENT

A. Synthesis of CsPbBr₃ perovskite nanowires

CsPbBr₃ nanowires are synthesized by chemical vapor deposition in a horizontal tube furnace from CsBr and PbBr₂ powders with a molar ratio of 2:1. Before the growth, we need to remove the air in the tube furnace followed by a 200 sccm flow of nitrogen for 10 min, and then we can increase the temperature of the tube furnace to come up to 550° under atmospheric pressure, with a nitrogen flow controlled at 20 sccm. After 5 min of reaction, we let the system return to room temperature naturally.

B. Optical measurement

The time-resolved photoluminescence (TRPL) studies are based on a confocal μ PL system (WITec, alpha-300). The excitation sources for single-photon pumped lasing and two-photon pumped lasing are a pulsed laser operated at 470 nm (100 fs, 1 kHz) and 800 nm (100 fs, 1 kHz), respectively. Excitation pulses at 800 nm are generated by a mode-locked Ti:sapphire laser (Tsunami) operating at 800 nm (pulse width 100 fs, repetition rate 80 MHz) amplified by a regenerative amplifier (Spitfire Ace 100, 1 kHz). Excitation pulses at 470 nm are converted from the pulses

at 800 nm introduced into an optical parameter amplifier (OPA, TOPAS Prime). The lasing signal is collected by an objective (50 \times , 0.55 NA). The power-dependent TRPL is detected by a streak camera system (Hamamatsu, C10910). All optical experiments are performed at room temperature.

III. RESULT AND DISCUSSION

First, we study the lasing dynamics of a single CsPbBr₃ nanowire by one-photon excitation with a laser wavelength of 470 nm at room temperature [Fig. 1(a)]. The CsPbBr₃ nanowires are synthesized by chemical vapor deposition as described in our previous publications [30,31]. The investigated nanowire is about 17 μ m long with a diameter of about 500 nm. At an excitation fluence below the lasing threshold, the time-resolved PL spectra show a nearly constant peak at approximately 2.325 eV with the PL dynamics exceeding the 700-ps time window [Fig. 1(b)], similar to the emission behavior from other CsPbBr₃ nanostructures [11]. Such spontaneous emission is considered mainly from the excitonic state of the CsPbBr₃ nanostructures, due to their reported exciton-binding energies larger than the thermal energy as well as the close distance between the emission and the first excitonic absorption peaks [8,32]. With an excitation fluence above the lasing threshold, intense green light is emitted from two end faces of the nanowire, as shown in the bright field optical image [Fig. 1(c)]. The time-resolved stimulated-emission spectra are collected by a streak camera for different excitation fluences above the lasing threshold [Fig. 1(a)], varying from 15.7 to 26.4 μ J cm⁻² (corresponding to a carrier density of several tens of 10²³ m⁻³ that exceeds the critical Mott density [29]). Each single streak-camera image is a two-dimensional plot of autoscaled emission intensity as a function of the wavelength and the decay time. The plotted time window is 40 ps as indicated by the white arrow. For laser excitations over the threshold, distinct lasing modes can be observed, which are labeled as mode A to mode E, corresponding to the emissions from high to low photon energy. These lasing modes are assigned to the longitudinal modes of the cavity defined by the nanowire facets at each end. The dashed lines in Fig. 1(a) mark the peak position as observed for low excitation fluence. Clearly, with increasing laser power, the same lasing mode shifts to higher photon energy. We plot the peak position of these lasing modes obtained from time-integrated spectra as a function of excitation laser power in Fig. 1(d). All individual lasing modes show about 2 meV blueshift (also see Fig. S1 within the Supplemental Material [33]), which agrees with previous observations from nanowire lasing in the literature and can be simply interpreted by the reduction of the refractive index with an increase of the carrier density. Note that all the lasing peaks developed under those excitation conditions appear only on the

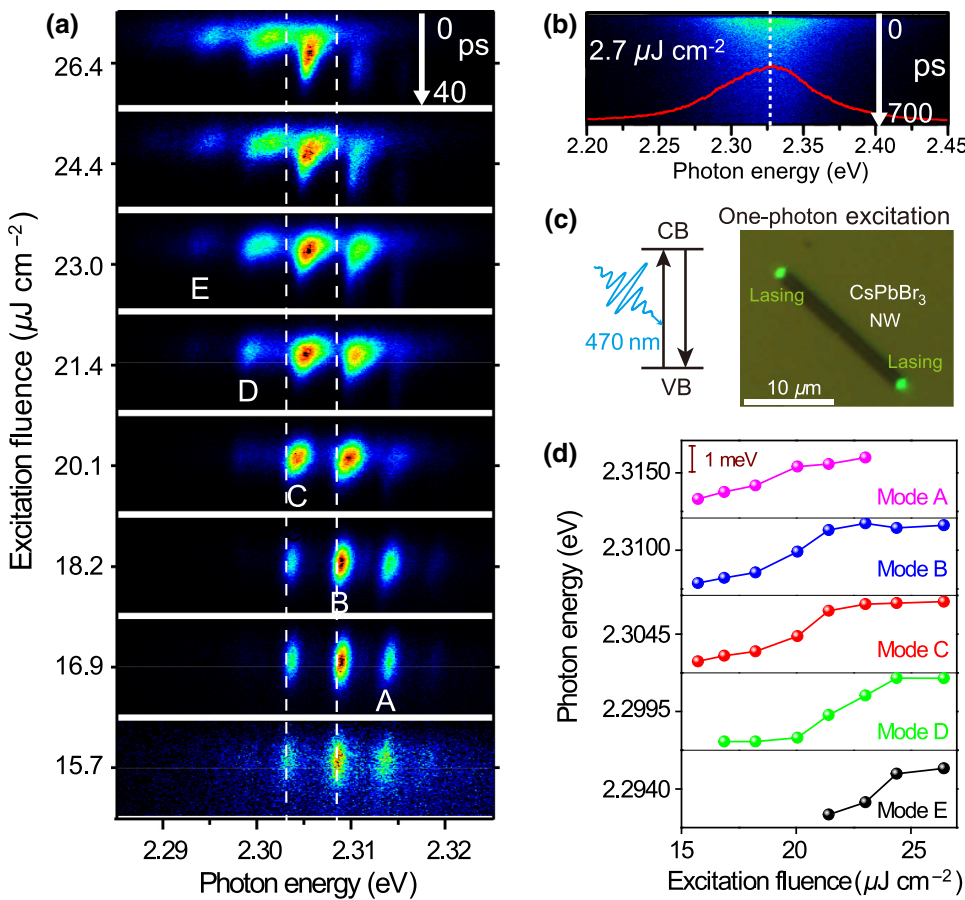


FIG. 1. (a) Streak-camera images of the lasing emission from the CsPbBr₃ nanowire under 470-nm fs pulse laser excitation with different excitation fluences at room temperature. For each image, the whole vertical axis range corresponds to the time window of 40 ps. Five discrete lasing modes are labeled with A to E. Dashed lines indicate the positions of the initial peaks of modes B and C at the lowest excitation fluence. (b) Streak-camera image of the spontaneous emission from the CsPbBr₃ nanowire under 470-nm fs pulse laser excitation with an excitation fluence of $2.7 \mu\text{J cm}^{-2}$ at room temperature. The vertical axis range corresponds to the time window of 700 ps. The red curve shows the time-integrated PL spectrum over the time window. (c) Bright-field optical image of the investigated nanowire and the lasing emission from two ends under wide-field illumination. (d) Peak position of the lasing modes as a function of excitation fluence. The vertical bar of 1 meV is shared in all plots.

lower-energy side of the PL spectrum, indicating the transition from the excitonic state to the EHP state that leads to the observed lasing, as reported for other semiconductor nanostructures [22,24,34–37]. Other reported lasing mechanisms such as exciton or exciton-polariton lasing [10,38,39] can be reasonably excluded in the present study, due to the applied excitation density exceeding the exciton Mott density for stabilizing the excitons. The FWHM of the lasing mode becomes broader as the excitation fluence increases [Fig. 1(a)], normally due to the more prominent scattering of the carriers as well as the heat effect. Moreover, with increasing the excitation fluence, we also observe the mode competition behavior together with the redshift of the whole gain profile [Fig. 1(a), also see Fig. S1 within the Supplemental Material [33]], as indicated by the appearance of modes D and E and the dwindling of mode A. That is, under a higher-power excitation, the appearance or strengthening of the laser mode at lower energy is accompanied by the quenching of laser mode at high photon energy. Such an obvious redshift of the gain profile suggests the band-gap renormalization with the carrier density as well as a further signature of the existence of EHP state [40,41] in the CsPbBr₃ nanowire.

To elucidate the photogenerated carrier and dynamics in the lasing process in CsPbBr₃ nanowires in more detail,

time-resolved emission spectra under different excitation conditions are systematically analyzed. For one-photon excitation with the recorded lowest ($15.7 \mu\text{J cm}^{-2}$) and the highest ($26.4 \mu\text{J cm}^{-2}$) fluences above the lasing threshold, the spectra collected within about the first 30 ps with 3-ps interval are shown in Figs. 2(a) and 2(b), respectively. The observed lasing modes show redshifted peak positions within the monitored time delay [Fig. 2(c)], which is also observed at other high excitation fluences (see Fig. S2 within the Supplemental Material [33]). The redshift of the lasing peak can be interpreted by the change of the effective refractive index of the material as described before, which is related to the carrier density with the elapsed time. Compared to the photogenerated high density right after the initial excitation, the carrier density decreases with the consummation to photon emission with further time delay, which leads to a slight increase of the refractive index n_r . Thus, we observe the redshifted cavity lasing modes E_i since $E_i \propto (1/n_r)$ in a Fabry-Perot cavity [42]. The redshift of the lasing modes at high excitation fluence is more obvious than that at low excitation fluence (also shown in Fig. S2 within the Supplemental Material [33]). This phenomenon is probably due to the larger carrier-density gradient with time delay under high excitation fluences, resulted by the more frequent collision of the carriers and

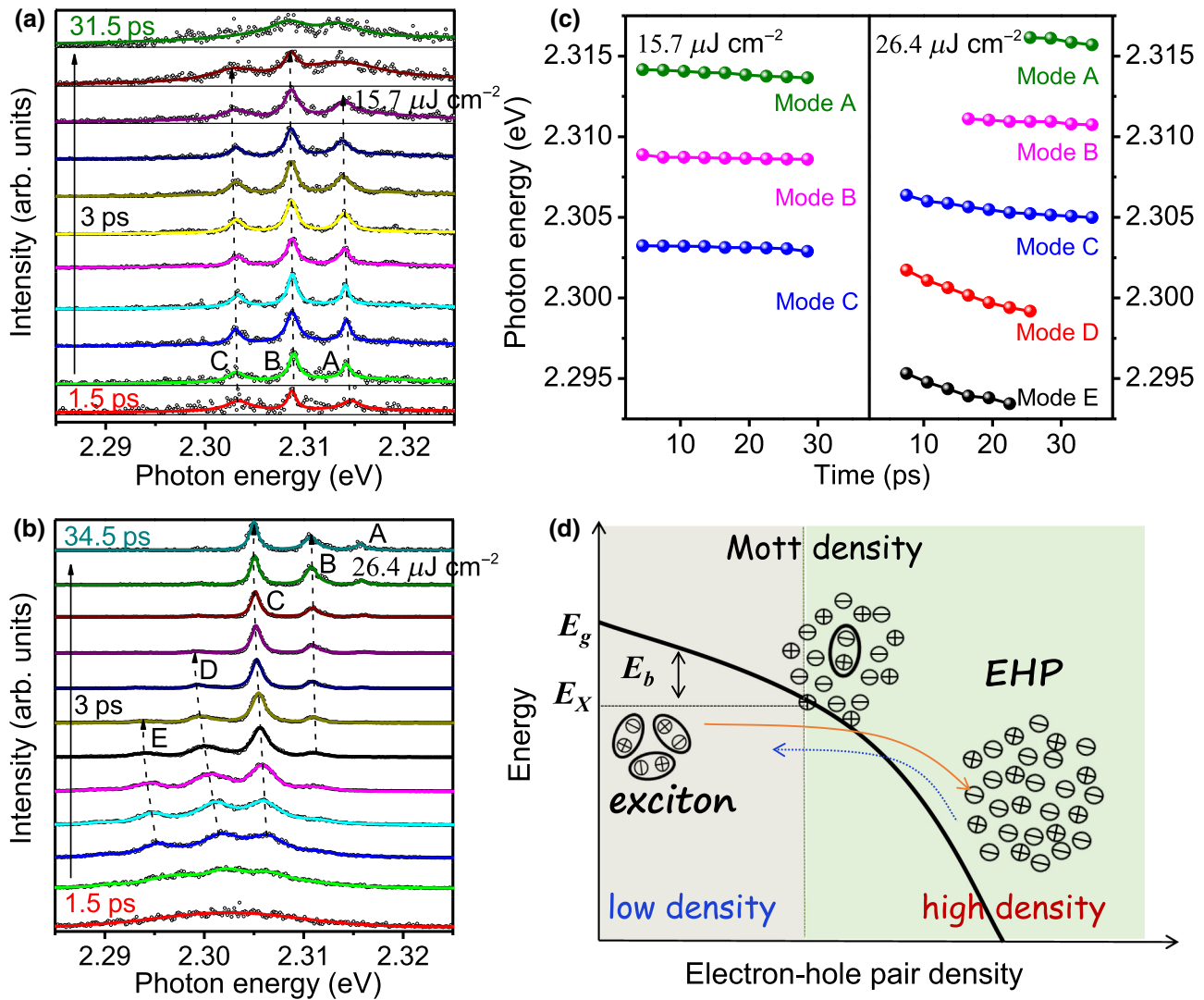


FIG. 2. (a),(b) Time-resolved emission spectra with different time delays from the one-photon excited CsPbBr₃ nanowire under the excitation fluences of 15.7 and 26.4 $\mu\text{J cm}^{-2}$. Solid lines are fitted spectra. Lasing modes are labeled (A, B, ...) in the figures. Dashed arrows indicate the variation of emission peak position with time elapsed. (c) Peak position of the lasing modes as a function of time delay derived from (a) and (b). (d) Physical model of the interplay and reversible transitions between the excitonic and EHP states. E_g , band-gap energy; E_X , exciton energy; E_b , exciton-binding energy; and EHP, electron-hole plasma.

thus faster decay of the carrier density. Another interesting phenomenon is that the lasing gain profile also shifts with time delay. At high excitation fluence, the whole gain profile shows an obvious blueshift with time evolution [Fig. 2(b)], also shown in cases at other high excitation fluences (see Fig. S2 within the Supplemental Material [33]). Such a blueshift of the gain profile with time delay implies an opposite direction of the process observed in Fig. 1(a), i.e., a redshift of the gain profile as the excitation fluence increases, both of which point to the carrier-density dependence of the optical gain as clarified in more detail below. One may be aware that at high excitation fluence [26.4 $\mu\text{J cm}^{-2}$, Fig. 2(b)], the initial spectrum is broad with no clear peaks and discrete lasing modes only emerge after

several ps, which is very likely due to the higher hot carrier density and thus a longer phonon-related cooling process to establish the lasing modes under those high excitation conditions [34–37]. At the recorded lowest excitation fluence above the lasing threshold [15.7 $\mu\text{J cm}^{-2}$, Fig. 2(a)], the blueshift of the gain profile with time delay is less prominent, and the lasing modes eventually evolve to an asymmetrically broad emission spectrum with its higher-energy side extending to the peak position (2.325 eV) of the excitonic emission, implying a back transition from the EHP state to the original excitonic state due to the decreased carrier density with time delay.

Combining the results from Figs. 1 and 2, a physical model is applied to qualitatively explain the observed

phenomena. As shown in Fig. 2(d), it is well known that the band gap (E_g) in semiconductors tends to decrease as the electron-hole pair density increases due to the exchange and correlation effects [20], the so-called band-gap renormalization. Whereas, below the Mott density, the absolute energy of the lowest exciton (E_X) is roughly maintained as the electron-hole pair density increases, owing to the almost complete compensation of the band-gap renormalization effect and the screening effect of the Coulomb attraction in the exciton. As a result, at low excitation fluence (i.e., low electron-hole pair density) below the Mott density, the optical properties of the low-dimensional materials are principally determined by the photogenerated excitons, which are good quasiparticles in this regime. This explains the optical behavior of the CsPbBr_3 nanowire at low excitation fluence below the lasing threshold, with the spontaneous PL emission dominated by the excitonic state [Fig. 1(b)]. However, on the other side, the exciton binding energy (E_b) gradually decreases because of the screening effect and the possible phase-space filling effect as increasing the excitation fluence, which could eventually vanish at the Mott density where the curves of E_g and E_X cross with each other [20]. Consequently, a transition from the

excitonic state to the EHP state occurs at the Mott density, with the EHP band redshifts to the longer wavelength as compared to the exciton band. With further increasing the excitation fluence above the Mott density, the population inversion between the conduction and valence bands may be satisfied, leading to lasing originating from the EHP state. This is exactly what is found in the CsPbBr_3 nanowire under excitation fluences above the lasing threshold (exceeding the Mott density), with all the lasing modes situated on the lower-energy side of the excitonic emission spectrum instead of the central region with the highest oscillation strength [Fig. 1(a)], suggesting the transition from the excitonic state to the EHP state for the observed lasing. In this high-density regime, the gradual redshift of the gain profile in the CsPbBr_3 nanowire with increasing the excitation fluence can be rationally ascribed to the band-gap renormalization effect, in which the value of the band gap reduces monotonically as the excitation density increases [Fig. 2(d)]. Such an explanation can also be applied to describe the time-evolution behavior of the gain profile shown in Figs. 2(a) and 2(b). As time elapses, the photogenerated carrier density decreases due to the recombination process, which shifts the band gap back to the

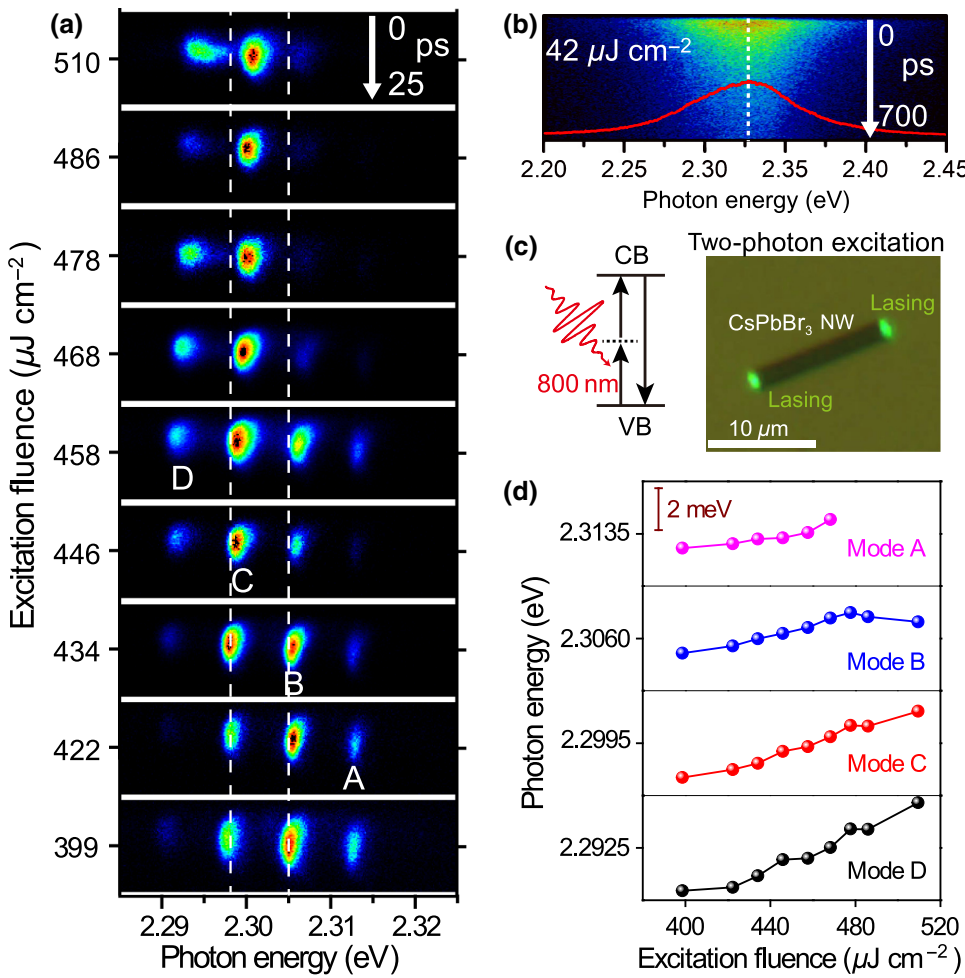


FIG. 3. (a) Streak-camera images (with a time window of 25 ps) of the lasing emission from a two-photon (800 nm) pumped CsPbBr_3 nanowire with different excitation fluences at room temperature. Four discrete lasing modes labeled with A to D are observed. (b) Streak-camera image of the spontaneous emission from the CsPbBr_3 nanowire pumped at 800 nm with an excitation fluence of $42 \mu\text{J cm}^{-2}$ at room temperature. The vertical axis range corresponds to the time window of 700 ps. The red curve shows the time-integrated PL spectrum over the time window. (c) Bright-field optical image of the investigated nanowire with the lasing emission from the end faces under two-photon wide-field illumination. (d) Peak position of the lasing modes as a function of excitation fluence. The vertical bar of 2 meV is shared in all plots.

higher energies and thus results in the blueshift of the gain profile with time delay [Fig. 2(b)]. At the recorded lowest excitation fluence above the lasing threshold [Fig. 2(a)], the photogenerated carrier density seems to diminish even below the critical value for EHP formation as time elapses, with a sudden phase transition from a collective EHP state to an excitonic state that leads to the observed broad emission band eventually. These phenomena demonstrate the interplay and reversible transitions between the excitonic and EHP states during the stimulated-emission process in the CsPbBr_3 nanowire at room temperature.

Carrier dynamics during lasing is also studied via two-photon pumped lasing from single nanowires, where the sample is excited by simultaneous absorption of two low-energy photons. Due to the nature of the two-photon

process and the smaller absorption coefficient, the lasing threshold of two-photon pumped lasing is about 1 order of magnitude higher than that of one-photon lasing. We show time- and photon-energy-resolved streak-camera images of two-photon (800 nm) pumped lasing emission with excitation fluences above the threshold varying from 399 to $510 \mu\text{J cm}^{-2}$ [Fig. 3(a)]. Similar to the one-photon pumped lasing, strong green-light emission from two ends of the $12\text{-}\mu\text{m}$ -long nanowire is observed [Fig. 3(c)]. Compared to the time scale of the one-photon excited dynamics, two-photon pumped carrier dynamics in general happen at a shorter time scale. In Fig. 3(a), the plotted time window is 25 ps. Four discrete lasing modes labeled as A to D can be observed. The dashed lines in Fig. 3(a) mark the peak position of mode C and mode D for the low excitation fluence.

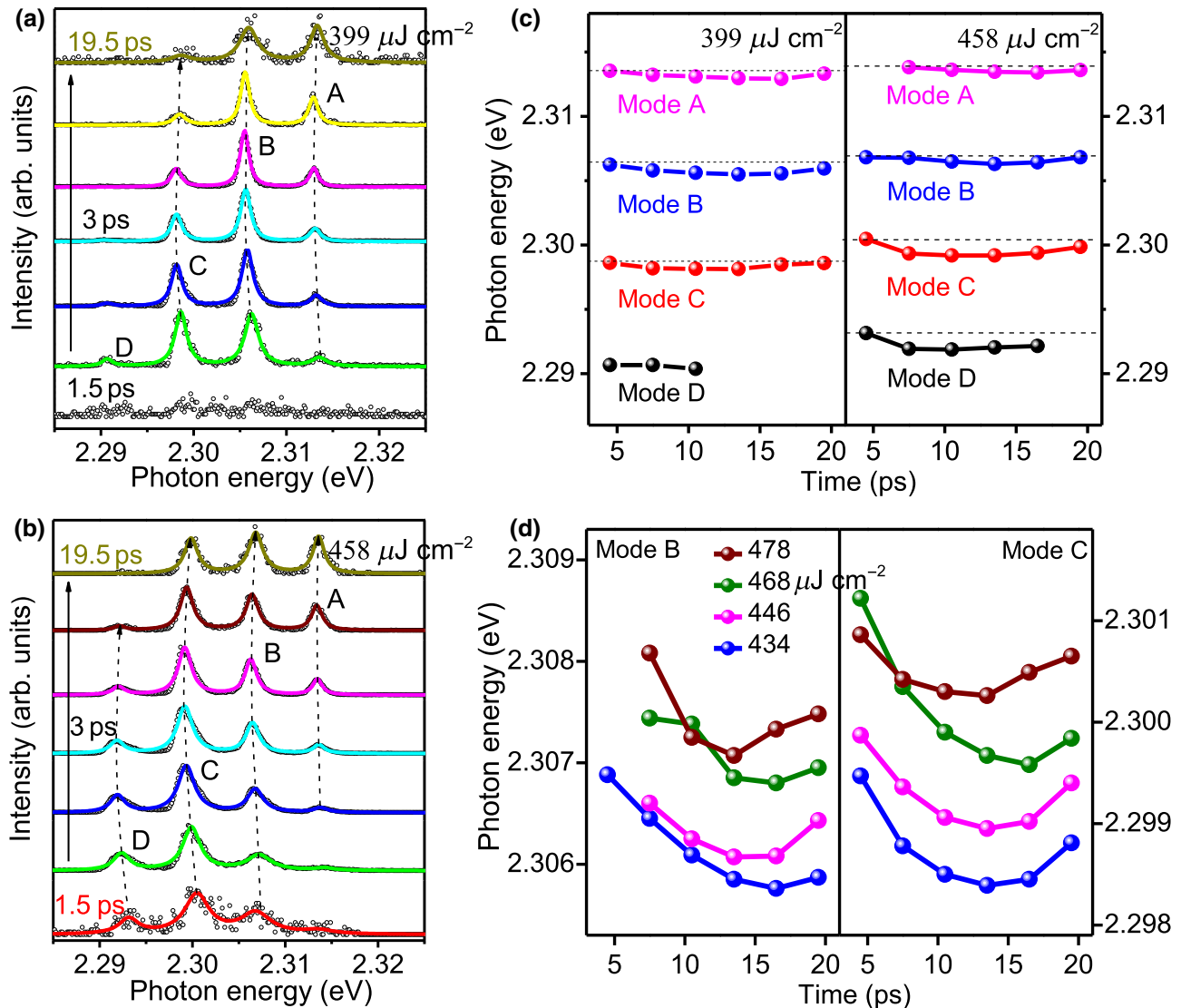


FIG. 4. (a), (b) Time-resolved lasing emission spectra with different time delays from the two-photon (800 nm) excited CsPbBr_3 nanowire under the excitation fluences of 399 and $458 \mu\text{J cm}^{-2}$. (c) Peak position of the lasing modes A to D as a function of time delay derived from (a) and (b). (d) Peak position of the lasing modes B and C as a function of time delay under other excitation fluences.

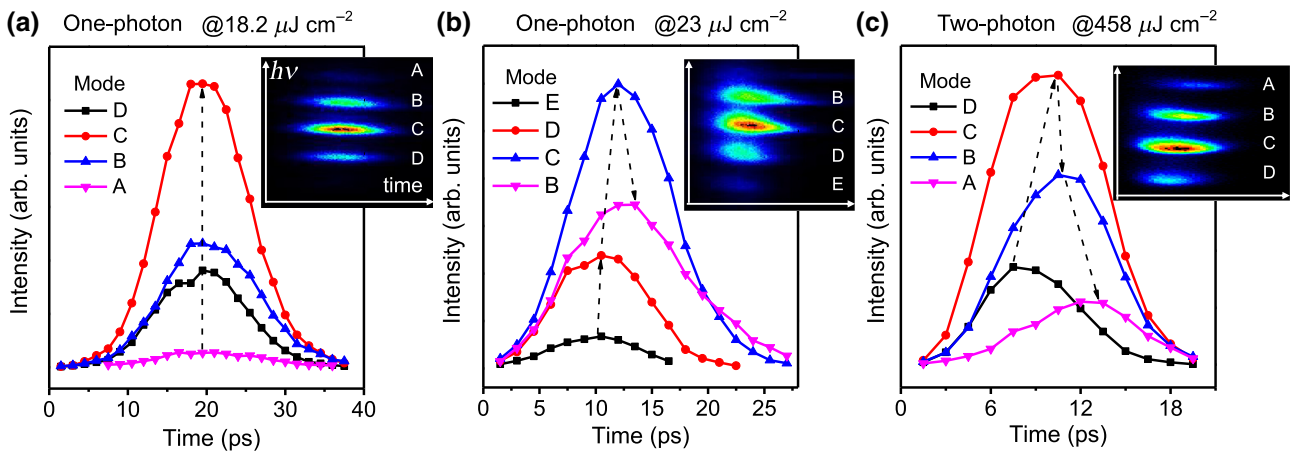


FIG. 5. (a)–(c) Emission intensity of different lasing modes for different excitation conditions as a function of time delay. Insets show respective streak-camera images with horizontal time axis and vertical photon-energy axis. For one-photon excitation with $18.2 \mu\text{J cm}^{-2}$ (a), all four lasing modes start and last for almost the same period of time. For one-photon excitation with a higher excitation fluence of $23 \mu\text{J cm}^{-2}$, the high-photon-energy mode B reaches its maximal intensity last, as indicated by the dashed arrows in (b). A clear trend with the low-photon-energy lasing mode starting first and high-photon-energy mode starting last is observed from the nanowire under two-photon excitation with excitation fluence of $458 \mu\text{J cm}^{-2}$ (c).

Similar to the one-photon excitation process, the lasing modes show about 3–4 meV blueshift due to the reduced refractive index with increasing excitation fluence. The peak position as a function of excitation fluence is plotted in Fig. 3(d). Meanwhile, as the case in one-photon excitation, all the lasing modes develop only on the lower-energy side of the excitonic emission band [Figs. 3(a) and 3(b)], meaning the transition from the excitonic state to the EHP state for lasing also occurring in the two-photon excitation. Moreover, with increasing excitation fluence, we also observe mode competition together with the redshift of the whole gain profile, owing to the band-gap renormalization effect as stated above.

Besides the redshift of the gain profile with increasing the excitation fluence, a blueshift of the gain profile with time delay should also be expected in the two-photon excitation, according to the former discussion. Figures 4(a) and 4(b) show the temporal evolution of the lasing spectra under two-photon pumping with the excitation fluences of 399 and $458 \mu\text{J cm}^{-2}$. In general, compared to the one-photon process, all lasing modes decay much faster in the two-photon process. Discrete peaks appear after a few ps. As time elapses, the low-energy peak mode declines and the high-energy peak mode emerges and enhances. This is clear evidence of the blueshift of the lasing gain profile with time delay, which can be assigned to the recovery of the renormalized band gap as the carrier density decreases with time, like the case in one-photon excitation. Interestingly, unlike the continuous redshift of individual lasing modes under one-photon excitation [Fig. 2(c)], the peak positions of the lasing modes show an initial redshift and later blueshift tendency [Fig. 4(c)]. These phenomena are observed at other excitation fluences as shown in Fig. 4(d).

(corresponding time-resolved lasing emission spectra are shown in Fig. S3 within the Supplemental Material [33]). Clearly, these phenomena are the result of the combination effects from the blueshift of the gain profile and the increase of refractive index with time delay [43], which also implies the different competition behavior between the recovery of the renormalized band gap and the changes of the refractive index in one-photon and two-photon excitation. In addition, the signal-to-noise ratio and resolution of the streak-camera images under two-photon excitation are much better than those under one-photon excitation, showing the potential applications in imaging as well as in nonlinear optics based on the studied CsPbBr_3 nanowires.

Due to the shift of the gain profile with time, under the same excitation condition different lasing modes from the same cavity can start at different times. A careful examination of the excitation-fluence-dependent time-resolved streak-camera images [Figs. 1(a) and 3(a)] reveal the different building times for different lasing modes. Figure 5 compares the emission intensity profiles with time for three typical excitation conditions of one-photon $18.2 \mu\text{J cm}^{-2}$, $23 \mu\text{J cm}^{-2}$ and two-photon $458 \mu\text{J cm}^{-2}$. Dashed arrows indicate the intensity reaching its maximum for different modes. The corresponding two-dimensional time (horizontal axis) and photon-energy- ($h\nu$, vertical axis) resolved streak-camera images are shown as insets in Fig. 5. For one-photon excitation with $18.2 \mu\text{J cm}^{-2}$, the blueshift of the gain profile is less prominent and all four lasing modes A to D start and reach their maxima at almost the same period of time (around 20 ps), as indicated by the straight dashed arrow in Fig. 5(a). In contrast, under a higher excitation fluence of $23 \mu\text{J cm}^{-2}$, the dominant four modes B to E show a little different building-up time, as indicated

by the inclined dashed arrows in Fig. 5(b), revealing a blueshift of the gain profile with time delay. This phenomenon is much more dramatic for the lasing from the nanowire under two-photon excitation with excitation fluence of $458 \mu\text{J cm}^{-2}$ [Fig. 5(c)]. The much-titled lasing pattern in the inset streak camera and the arrows in the intensity profiles clearly demonstrate this trend, with the low-photon-energy lasing mode starting first and high-photon-energy mode starting last, giving clear evidence of the blueshift of the gain profile with time delay. As discussed above, for the lasing originated from the EHP state, the gain profile shifts to blue with time since the renormalized band gap back shifts to higher energies as the carrier density decreases.

Earlier, lasing from the EHP state and the shift of its gain profile have been mostly studied in ZnO nanostructures [22,24,34,35,37], whereas such observations in perovskites are less reported [28,29]. CsPbBr₃ as an all-inorganic perovskite with typically long carrier lifetime, its carrier behavior may resemble those of conventional inorganic semiconductors to some extent and thus be favorable to observe an EHP under excitation. In fact, lasing from EHP state was recently found in CsPbBr₃ nanowires under one-photon excitation at liquid nitrogen temperature [29]. Here, we observe the lasing from EHP state in CsPbBr₃ nanowires under both one-photon and two-photon excitation at room temperature, and the microscopic processes involved in the stimulated emission with the interplay and reversible transitions between the excitonic and EHP states are revealed.

IV. CONCLUSION

In conclusion, carrier behaviors and dynamics of the stimulated emission in CsPbBr₃ single nanowires are studied by streak camera under power-dependent one-photon and two-photon excitations at room temperature. For one-photon pumped lasing, in general, we observe a blueshift of individual lasing modes with increasing excitation fluence and redshift of the modes with time decay, which can be interpreted by the carrier-density-dependent refractive-index changes. Meanwhile, a redshift of the lasing gain profile with increasing excitation fluence and a blueshift of the gain profile with time decay are observed, which can be ascribed to the changes of the band gap with carrier density and reveal the interplay and reversible transitions between the excitonic and EHP states in these nanowires. All these phenomena are also observed under two-photon excitation with better signal-to-noise ratio and resolution of the results. Our detailed carrier-dynamics studies can provide a complete and deeper understanding of the lasing mechanism and dynamics in lead halide nanowires and extend their applications in integrated photonics.

ACKNOWLEDGMENTS

The authors are grateful to the National Natural Science Foundation of China (Grants No. 91850116, No. 51772084, No. U19A2090, No. 51525202, and No. 21703059), the Hunan Provincial Natural Science Foundation of China (Grant No. 2018RS3051).

M.H. and Y.J. contributed equally to this work.

-
- [1] M. A. Green, A. Ho-Baillie, and H. J. Snaith, The emergence of perovskite solar cells, *Nat. Photonics* **8**, 506 (2014).
 - [2] Q. Lin, A. Armin, R. C. R. Nagiri, P. L. Burn, and P. Meredith, Electro-optics of perovskite solar cells, *Nat. Photonics* **9**, 106 (2015).
 - [3] Y. Cao *et al.*, Perovskite light-emitting diodes based on spontaneously formed submicrometre-scale structures, *Nature* **562**, 249 (2018).
 - [4] K. Lin, J. Xing, L. N. Quan, F. P. G. de Arquer, X. Gong, J. Lu, L. Xie, W. Zhao, D. Zhang, C. Yan, W. Li, X. Liu, Y. Lu, J. Kirman, E. H. Sargent, Q. Xiong, and Z. Wei, Perovskite light-emitting diodes with external quantum efficiency exceeding 20 per cent, *Nature* **562**, 245 (2018).
 - [5] H. Zhu, Y. Fu, F. Meng, X. Wu, Z. Gong, Q. Ding, M. V. Gustafsson, M. T. Trinh, S. Jin, and X. Y. Zhu, Lead halide perovskite nanowire lasers with low lasing thresholds and high quality factors, *Nat. Mater.* **14**, 636 (2015).
 - [6] S. W. Eaton, M. Lai, N. A. Gibson, A. B. Wong, L. Dou, J. Ma, L.-W. Wang, S. R. Leone, and P. Yang, Lasing in robust cesium lead halide perovskite nanowires, *Proc. Natl. Acad. Sci.* **113**, 1993 (2016).
 - [7] H. Zhou, S. Yuan, X. Wang, T. Xu, X. Wang, H. Li, W. Zheng, P. Fan, Y. Li, L. Sun, and A. Pan, Vapor growth and tunable lasing of band Gap engineered cesium lead halide perovskite micro/nanorods with triangular cross section, *ACS Nano* **11**, 1189 (2017).
 - [8] Q. Zhang, R. Su, X. Liu, J. Xing, T. C. Sum, and Q. Xiong, High-Quality whispering-gallery-mode lasing from cesium lead halide perovskite nanoplatelets, *Adv. Funct. Mater.* **26**, 6238 (2016).
 - [9] B. R. Sutherland and E. H. Sargent, Perovskite photonic sources, *Nat. Photonics* **10**, 295 (2016).
 - [10] T. J. S. Evans, A. Schlaus, Y. Fu, X. Zhong, T. L. Atallah, M. S. Spencer, L. E. Brus, S. Jin, and X.-Y. Zhu, Continuous-Wave lasing in cesium lead bromide perovskite nanowires, *Adv. Opt. Mater.* **6**, 1700982 (2018).
 - [11] X. Wang, H. Zhou, S. Yuan, W. Zheng, Y. Jiang, X. Zhuang, H. Liu, Q. Zhang, X. Zhu, X. Wang, and A. Pan, Cesium lead halide perovskite triangular nanorods as high-gain medium and effective cavities for multiphoton-pumped lasing, *Nano Res.* **10**, 3385 (2017).
 - [12] Y. Xu, Q. Chen, C. Zhang, R. Wang, H. Wu, X. Zhang, G. Xing, W. W. Yu, X. Wang, Y. Zhang, and M. Xiao, Two-Photon-Pumped perovskite semiconductor nanocrystall lasers, *J. Am. Chem. Soc.* **138**, 3761 (2016).
 - [13] Y. Wang, X. Li, X. Zhao, L. Xiao, H. Zeng, and H. Sun, Nonlinear absorption and Low-threshold multiphoton

- pumped stimulated emission from All-inorganic perovskite nanocrystals, *Nano Lett.* **16**, 448 (2016).
- [14] Y. Fu, H. Zhu, C. C. Stoumpos, Q. Ding, J. Wang, M. G. Kanatzidis, X. Zhu, and S. Jin, Broad wavelength tunable robust lasing from single-crystal nanowires of cesium lead halide perovskites (CsPbX_3 , $X = \text{Cl}, \text{Br}, \text{I}$), *ACS Nano* **10**, 7963 (2016).
- [15] Y. Fu, H. Zhu, J. Chen, M. P. Hutzinger, X. Y. Zhu, and S. Jin, Metal halide perovskite nanostructures for optoelectronic applications and the study of physical properties, *Nat. Rev. Mater.* **4**, 169 (2019).
- [16] H. Zhu, K. Miyata, Y. Fu, J. Wang, P. P. Joshi, D. Niesner, K. W. Williams, S. Jin, and X.-Y. Zhu, Screening in crystalline liquids protects energetic carriers in hybrid perovskites, *Science* **353**, 1409 (2016).
- [17] K. Miyata, T. L. Atallah, and X.-Y. Zhu, Lead halide perovskites: Crystal-liquid duality, phonon glass electron crystals, and large polaron formation, *Sci. Adv.* **3**, 1469 (2017).
- [18] Y. Jiang, X. Wang, and A. Pan, Properties of excitons and photogenerated charge carriers in metal halide perovskites, *Adv. Mater.* **31**, 6671 (2019).
- [19] R. Agarwal, C. J. Barrelet, and C. M. Lieber, Lasing in single cadmium sulfide nanowire optical cavities, *Nano Lett.* **5**, 917 (2005).
- [20] C. F. Klingshirn, *Semiconductor Optics* (2007).
- [21] R. Huber, F. Tauser, A. Brodschelm, M. Bichler, G. Abstreiter, and A. Leitenstorfer, How many-particle interactions develop after ultrafast excitation of an electron-hole plasma, *Nature* **414**, 286 (2001).
- [22] S. Mitsubori, I. Katayama, S. H. Lee, T. Yao, and J. Takeda, Ultrafast lasing due to electron-hole plasma in ZnO nano-multipods, *J. Phys.: Condens. Matter* **21**, 064211 (2009).
- [23] T. Shih, E. Mazur, J.-P. Richters, J. Gutowski, and T. Voss, Ultrafast exciton dynamics in ZnO: Excitonic versus electron-hole plasma lasing, *J. Appl. Phys.* **109**, 043504 (2011).
- [24] J. Dai, C. X. Xu, P. Wu, J. Y. Guo, Z. H. Li, and Z. L. Shi, Exciton and electron-hole plasma lasing in ZnO dodecagonal whispering-gallery-mode microcavities at room temperature, *Appl. Phys. Lett.* **97**, 011101 (2010).
- [25] T. Nakamura, K. Firdaus, and S. Adachi, Electron-hole plasma lasing in a ZnO random laser, *Phys. Rev. B* **86**, 205103 (2012).
- [26] E. Hendry, M. Koeberg, and M. Bonn, Exciton and electron-hole plasma formation dynamics in ZnO, *Phys. Rev. B* **76**, 045214 (2007).
- [27] C. Klingshirn, R. Hauschild, J. Fallert, and H. Kalt, Room-temperature stimulated emission of ZnO: Alternatives to excitonic lasing, *Phys. Rev. B* **75**, 115203 (2007).
- [28] M. Saba, M. Cadelano, D. Marongiu, F. Chen, V. Sarritzu, N. Sestu, C. Figus, M. Aresti, R. Piras, A. Geddo Lehmann, C. Cannas, A. Musinu, F. Quochi, A. Mura, and G. Boniovanni, Correlated electron-hole plasma in organometal perovskites, *Nat. Commun.* **5**, 5049 (2014).
- [29] A. P. Schlaus, M. S. Spencer, K. Miyata, F. Liu, X. Wang, I. Datta, M. Lipson, A. Pan, and X. Y. Zhu, How lasing happens in CsPbBr_3 perovskite nanowires, *Nat. Commun.* **10**, 265 (2019).
- [30] M. Shoaib, X. Zhang, X. Wang, H. Zhou, T. Xu, X. Wang, X. Hu, H. Liu, X. Fan, W. Zheng, T. Yang, S. Yang, Q. Zhang, X. Zhu, L. Sun, and A. Pan, Directional growth of ultralong CsPbBr_3 perovskite nanowires for high-performance photodetectors, *J. Am. Chem. Soc.* **139**, 15592 (2017).
- [31] X. Wang, M. Shoaib, X. Wang, X. Zhang, M. He, Z. Luo, W. Zheng, H. Li, T. Yang, X. Zhu, L. Ma, and A. Pan, High-Quality In-plane aligned CsPbX_3 perovskite nanowire lasers with composition dependent strong exciton-photon coupling, *ACS Nano* **12**, 6170 (2018).
- [32] L. Protesescu, S. Yakunin, M. I. Bodnarchuk, F. Krieg, R. Caputo, C. H. Hendon, R. X. Yang, A. Walsh, and M. V. Kovalenko, Nanocrystals of cesium lead halide perovskites (CsPbX_3 , $X = \text{Cl}, \text{Br}$, and I): Novel optoelectronic materials showing bright emission with wide color gamut, *Nano Lett.* **15**, 3692 (2015).
- [33] See Supplemental Material at <http://link.aps.org supplemental/10.1103/PhysRevApplied.13.044072> for the steady-state spectra, transient spectra below the lasing threshold, and transient spectra above the lasing threshold.
- [34] J. Fallert, F. Stelzl, H. Zhou, A. Reiser, K. Thonke, R. Sauer, C. Klingshirn, and H. Kalt, Lasing dynamics in single ZnO nanorods, *Opt. Express* **16**, 1125 (2008).
- [35] C. Klingshirn, J. Fallert, H. Zhou, J. Sartor, C. Thiele, F. Maier-Flaig, D. Schneider, and H. Kalt, 65 years of ZnO research - old and very recent results, *Phys. Status Solidi B* **247**, 1424 (2010).
- [36] S. M. Peng, G. C. Xing, and Z. K. Tang, Hot electron-hole plasma dynamics and amplified spontaneous emission in ZnTe nanowires, *Nanoscale* **9**, 15612 (2017).
- [37] N. Arai, J. Takeda, H. J. Ko, and T. Yao, Dynamics of high-density excitons and electron-hole plasma in ZnO epitaxial thin films, *J. Lumin.* **119**, 346 (2006).
- [38] K. Park, J. W. Lee, J. D. Kim, N. S. Han, D. M. Jang, S. Jeong, J. Park, and J. K. Song, Light-Matter interactions in cesium lead halide perovskite nanowire lasers, *J. Phys. Chem. Lett.* **7**, 3703 (2016).
- [39] R. Su, C. Diederichs, J. Wang, T. C. H. Liew, J. X. Zhao, S. Liu, W. G. Xu, Z. H. Chen, and Q. H. Xiong, Room-Temperature polariton lasing in All-inorganic perovskite nanoplatelets, *Nano Lett.* **17**, 3982 (2017).
- [40] R. Zimmermann, Many Particle Theory of Highly Excited Semiconductors (1988).
- [41] C. Klingshirn, Zno: Material, physics and applications, *ChemPhysChem* **8**, 782 (2007).
- [42] J. C. Johnson, H. Q. Yan, P. D. Yang, and R. J. Saykally, Optical cavity effects in ZnO nanowire lasers and waveguides, *J. Phys. Chem. B* **107**, 8816 (2003).
- [43] J. Takeda, H. Jinnouchi, S. Kurita, Y. F. Chen, and T. Yao, Dynamics of photoexcited high density carriers in ZnO epitaxial thin films, *phys. Status solidi (b)* **229**, 877 (2002).